Nanoscale

Accepted Manuscript

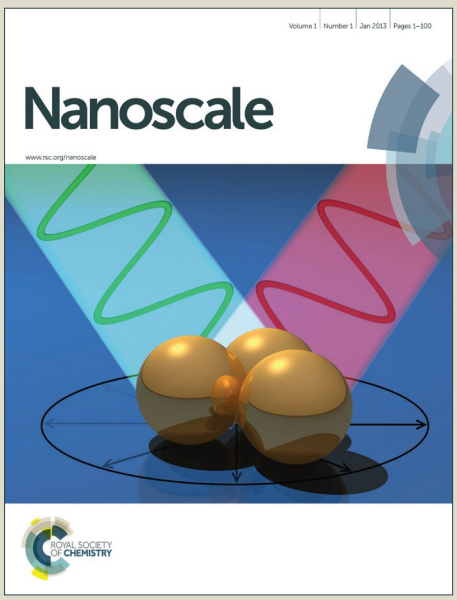

ROYAL SOCIETY OF CHEMISTRY

www.rsc.org/nanoscale

Antibacterial Au nanostructured surfaces

Songmei Wu,[1,2]* Flavia Zuber[3], Juergen Brugger[2], Katharina Maniura-Weber[3], and Qun Ren[3]*

[1] School of Science, Beijing Jiaotong University, No.3 Shangyuancun, Haidian District, Beijing, 100044, P. R. China

[2] Microsystems Laboratory, École Polytechnique Fédérale de Lausanne, Station 17, 1015 Lausanne, Switzerland

[3] Laboratory for Biointerfaces, Empa, Swiss Federal Laboratories for Materials Science and Technology, Lerchenfeldstrasse 5, 9014 St. Gallen, Switzerland.

Correspondence: smwu@bjtu.edu.cn; qun.ren@empa.ch

Keywords: Au nanostructures, fabrication of nanosurfaces, electrodeposition, antibacterial surfaces

ABSTRACT: We present here a technological platform for engineering Au nanotopographies by templated electrodeposition for antibacterial surfaces. Three different types of nanostructures were fabricated: nanopillars, nanorings and nanonuggets. The nanopillars are the basic structures and are 50 nm in diameter and 100 nm in height. Particular arrangement of the nanopillars in various geometries formed nanorings and nanonuggets. Flat surfaces, rough substrate surfaces, and various nanostructured surfaces were compared for their abilities to attach and kill bacterial cells. *Methicillin-resistant Staphylococcus aureus*, a Gram-positive bacterial strain responsible for many infections in health care system, was used as the model bacterial strain. It was found that all the Au nanostructures, regardless their shapes, exhibited similarly excellent antibacterial property. The comparison of live cells attached to nanotopographic surfaces showed that the number of live *S. aureus* cells was < 1 % of that from flat and rough reference surfaces. Our micro/nanofabrication process is a scalable approach based on cost-efficient self-organization and provides potential for further developing functional surfaces to study the behavior of microbes on nanoscale topographies.

Introduction

Anti-microbial contamination of surfaces is a central challenge in medical and industrial applications. Conventional biochemical approaches rely on the coatings of biocidal substances such as silver and antibiotics. Despite their wide use in various fields, chemical toxicity, antimicrobial durability and antimicrobial resistance remain critical problems. Alternatively, biophysical approaches prevent bacterial contamination by either anti-adhesive repelling[1-8] or direct contact killing[9-13] via micro/nanoscale surface topographies. The biophysical approaches attract much research attention in last decade thanks to the development of nanotechnologies[8, 14-19]. Various nanotopographies such as ridges, ripples and nanowire brushes have been developed to modulate cell–surface interactions in order to reduce the cell adhesion on the surfaces[2, 4, 8, 18, 20]. Recently, nanopillar structures of natural cicada's wings were found to be deadly to *Pseudomonas aeruginosa* by mechanically tearing the attached cells apart[9, 10, 21]. Natural cicada wings are however only effective against Gram-negative cells[9]. Gram-positive cells are generally more rigid and more resistant to mechanical deformation as their peptidoglycan cell walls are 4-5 times thicker than those of the Gram-negative bacteria[22]. Inspired by the well-defined nanopillar structures of cicada's wings, several synthetic nanomaterials such as black silicon and TiO_2 nanowires which contain high aspect ratio sharp nanoprotrusions have been developed.[11, 12] For example, black silicon with high aspect ratio rigid nanoprotrusions has demonstrated efficient bactericidal performance against both Gram-negative and positive bacteria[11].

One major challenge for studying the interaction of bacteria with surface nanostructures is to establish a platform, which allows the modulation of structural parameters such as topography, density and aspect ratio. Metal materials are interesting as they have additional functionalities such as electrical response and optical properties like plasma resonance, and many of these

properties are closely linked with their nanoscale topographies. By taking Au as a proof of concept metal material, we present here a novel cost-efficient micro/nanofabrication platform based on self-organization for engineering various nanotopographies and study the structural effects on the antibacterial performance. Three different types of nanostructures: nanopillars, nanorings and nanonuggets were fabricated and compared for their abilities to attach and kill bacterial cells. We selected *Methicillin-resistant Staphylococcus aureus*, a Gram-positive bacterial strain responsible for many infections, as the model bacterial strain, and focused on the nanoscale morphological effects on the antibacterial performance. The bactericidal property of various nanotopographies was observed and evaluated by fluorescent microscopy, scanning electron microscope (SEM) and cell proliferation assays.

Results and discussion

Au nanotopographies.

Figure 1a shows the fabrication process of Au nanostructured surfaces, which are generated by electrodeposition in nanoporous alumina templates. First, thin films of W (400 nm) and Al (300 nm) were coated by sputtering and evaporation on a Si wafer. The W layer serves as the electrode for Al anodization. By anodization of the Al film, an alumina nanoporous template was then formed on the W layer. After selectively dissolving the porous template, the remaining W coated Si wafer serves as the reference W substrate (S1). The W surface was roughened at the nanometer scale during the Al anodization process. Various Au nanotopographies of nanopillar, nanoring and nanonugget (S2-S4) were fabricated by electrodeposition of Au in the alumina nanoporous template followed by template dissolution. Au nanorings and nanonuggets were

obtained by further modifying the surface structure of W using SF_6 plasma etching prior to Au electrodeposition. Plasma etching of W through the alumina nanoporous template generated large holes under the alumina nanopores[23]. During the etching process, the plasma also partially etched away the top alumina template, especially at the interface. These holes were connected with each other, forming various nanocavities in the W layer. As the nanopores in the alumina template were self-organized in a near-hexagonal pattern, both Au nanorings (S3) andnanonuggets (S4) were created on the substrate, but their morphologies still retain the features of the pillar structure. More details of the nanoporous templates for the formation of nanorings and nanonuggets are provided in the supporting materials (Figure S1-S3).

SEM characterization shown in Figure 1b illustrates various nanostructured morphologies: S1 is the W reference substrate with nanoscale roughness; S2 is the Au nanopillar structure. Typical nanopillars are ~ 50 nm in diameter and ~ 100 nm in height; S3 is the Au nanoring formed by single nanopillars; S4 is the nugget of Au nanopillars. The typical outer diameter of nanorings and nanonuggets is about 200 nm, with the height about 100 nm which is similar to that of the single pillars. Inset pictures are enlarged single structures. The surface coverage with nanostructures is nearly half of the sample area. The rest surface is similar to that of reference W substrate. The inhomogeneity of the surface nanostructures is due to the defects generated by relatively low degree of self-organization during the anodization of very thin Al film. The homogeneity can be improved by pre-patterning of Al surface before anodization.[24]

As the nanostructures are fabricated by Au electrodeposition directly on a metal layer (W), the adhesion is rather stable. These nanostructures remain well resolved after at least 3 months immersing in DI.

Au nanostructured surfaces are bactericidal.

To study the bactericidal properties of the nanostructured surfaces, each surface type was incubated with *S. aureus* for 2 h and the bacterial viability was then analyzed using fluorescent microscopy. The Syto9/PI staining, which measures bacterial viability as a function of cell membrane integrity, revealed strong bactericidal activity of all the well-defined Au nanostructures (nanopillars, nanorings and nanonuggets) compared to the W substrate only with nanoscale roughness. One example of comparison is shown in Figure 2: nearly all *S. aureus* cells are alive on the reference W substrate (S1, Figure 2a); on the contrary, most of them appear dead on the Au nanopillars covered W substrate (S2, Figure 2b). These results were further confirmed by SEM investigation. The morphology of the cells on the nanopillar structured surfaces was found to be significantly different from those on the rough surface of reference W substrate (Figure 2c). Cell deformation and cell rupture could be seen clearly for the cells on the nanopillar surfaces S2 (Figure 2d).

The principle for bactericidal activity of nanostructured surfaces is based on nanomechanics. The mechanical antibacterial properties of nanopatterned surfaces were first demonstrated for natural Cicada wings.[9] The wing surfaces are covered by a dense array of nanopillars with height of 200 nm and a spherical cap of 60 nm in diameter. A biophysical model was developed to provide

insight into the interactions between the bacterial cell and nanopillar structures[21]. In this macroscopic description, the bacterial surface is considered as a planar piece of a membrane (with certain stretching modulus) adsorbing on the nanopillars. Apart from the area in contact with the cap, the rest of the membrane is suspended between the nanopillars. The total free energy is the sum of energy gain due to cell-nanopillar cap adsorption, and energy loss associated with membrane deformation. It has been proposed that when the bacteria are brought close to the nanopatterned surfaces, their adhesion on the surface is driven by gravitational forces, Brownian motion or hydrodynamic forces[2]. The bacterial cell membrane tends to maximize the contact area with the nanotopographical features to gain surface energy.[9, 21] When the adsorption energy is negative, the stretching of the suspended region is higher than the stretching of the adsorbed region, leading to mechanical rupture of the cell membrane between nanopillars. The nanopillars actually do not pierce the membrane, but rather break the membrane between the nanopillars. This model indicates that the bactericidal mechanism is nano-mechanical and does not imply specific biological interactions.[21]

Our Au nanostructures displayed highly bactericidal efficiency for *S. aureus*, which is one of the Gram-positive pathogenic bacteria. Similar phenomena of cell deformation and rupture have been shown in earlier work of bactericidal property of natural cicada's wings. However, the nanopillar structure on cicada's wings was demonstrated bactericidal only for soft Gram-negative bacteria such as *Pseudomonas aeruginosa*, as Gram-positive cells have thicker cell membranes and are generally more rigid and more resistant to mechanical deformation[9]. Recently, it was reported that black Si also exhibited bactericidal property for Gram-positive bacteria[11]. The deformation and cell wall stress were enhanced with longer (500 nm) and more pronounced dense nanospikes of the black Si. Our Au nanostructures show high bactericidal

efficiency for relatively more rigid *S. aureus* cells with the dimension similar to cicada's wings. The observation suggests that apart from the structural dimensions, the material properties such as stiffness also influence the deformation stress of bacterial cell membranes.

Quantification of bactericidal efficiency by proliferation measurement.

As both optical microscope and SEM images provide limited view of quantification, the bactericidal efficiency of the reference and nanostructured surfaces with area of 1×1 cm^2 was quantitatively assessed and compared using a proliferation assay (Figure 3a). After cell attachment (step 1 and 2), the samples were rinsed and incubated in fresh medium (step 3 and 4). The supernatant was then taken for turbidity measurements to monitor the proliferation of the attached cells (step 5 and 6). It is an indirect method to quantify the bactericidal ability of the surface nanostructures. The less viable cells on sample surfaces, the longer time is needed to reach a specific OD value. This assay is advantageous over the classical plate-count assay because it measures the viable cells attached on a surface via growth kinetic instead of one time point measurement. The proliferation curves are compared in Figure 3b. The cells on the reference substrate reached an OD value of 0.35 after 12 hours, whereas the three nanostructured surfaces reached only an OD value of 0.15. The number of viable cells during the proliferation process was extrapolated for the OD value of 0.2 for all the samples (Figure. 3c). The assay showed that the viable cell number on all nanostructured surfaces significantly decreased 3 orders of magnitudes compared to that on the flat surfaces and rough reference substrate surfaces. On the basis of these numbers, the killing efficiency of different surfaces was calculated and summarized in Table 1. The number of killed cells was determined as the difference between the number of surviving cells and those remaining on the reference substrate control S1. The

bactericidal activities of these topologically related surfaces appear to be largely comparable; all three surfaces have killing efficiency of more than 99 % during the 2 h interaction for *S. aureus*. The proliferation measurement showed comparable antibacterial performance for various Au nanomorphologies. In our work, we developed a technological platform for engineering Au nanotopographies based on templated electro-deposition. The nanopillars are the basic structures and are 50 nm in diameter and 100 nm in height. The nanorings and nanonuggets were obtained by modifying the templates but they still retained the dimensional features of the pillar structure. For example, the nanoring is composed of single pillars, and the nanonugget has nanoprotrusion on the surface. The height and density of these nanomorphologies are similar, so the stretching degree and antibacterial properties are comparable. One may expect nanopillars having the best performance as they induce more deformation and stretching positions on the cell membrane. However, this difference is not significant statistically based on the T-test.

We have performed additional experiments by decreasing and increasing the height of the nanopillars. When the height of the pillar is only 50 nm, the ‘‘pillars’’ became more like ‘‘dots’’, the deformation of the cell membrane was reduced and therefor most S. aureus cells appeared alive. When the height of the pillar is about 400 nm, the stretching degree is large enough that nearly all the cells were dead. The data were provided in the supporting material (Figure. S4 and S5).

Conclusions

In conclusion, we have developed a novel technological platform for scalable electrodeposition of various Au nanostructures in various geometries on a W reference surface. Inspired by the nanopattern of natural cicada’s wings, nanopillar, nanoring and nanonugget were successfully

fabricated. By using *Methicillin-resistant S. aureus* as model bacterial strain, the bactericidal effect of *S. aureus* on various surface nanotopographies was demonstrated by fluorescent microscopy and scanning electron microscope. We have found that all the studied shapes of Au nanostructures demonstrate excellent antibacterial performance. Mechanical deformation of cell membranes was observed by SEM imaging on high aspect ratio structures. We also quantitatively evaluated the antibacterial performance by cell proliferation experiments. The number of live *S. aureus* cells on Au nanotopographic surfaces is 3 orders of magnitude lower than that from flat and rough reference surfaces. Our micro/nanofabrication process is a cost-efficient approach based on self-organization. Metal materials have additional advantages such as electrical response and optical properties like plasma resonance. Our findings may lead to a prospect for the development and scaling up of a new generation of electro-/optical- responsive antibacterial surfaces.

Experimental section

Chemicals and reagents. All chemicals and reagents were purchased from Sigma-Aldrich (Buchs, Switzerland), if not mentioned.

Fabrication of Au nanotopographies. Au nanotopographies were fabricated by electrodeposition of Au in nanoporous templates. At first, a conducting layer of 300 nm W was sputtered on a Si wafer. Then on the W layer another 400 nm of Al layer was evaporated. The top thin Al film was then anodized in phosphoric acid solution (6 wt % H_3PO_4) under 60 V using a Pt mesh as counter electrode. During the anodization process, the aluminum layer was oxidized to alumina with self-organized straight nanopore structures. Then the nanopores were slightly enlarged in H_3PO_4 solution for 30 min at pore opening rate of 0.5 nm/min. After thoroughly rinsing with DI water, the samples were dried under nitrogen. The structure of underneath W layer was modified by SF_6 plasma etching using RIE (Reactive Ion Etching) process in an STS Multiplex ICP (Inductively Coupled Plasma) etcher. By using the W layer as electrode, Au nanostructures were then electrodeposited inside the nanocavities. Finally, the Au nanostructures were released after selectively dissolving the alumina template in H_3PO_4 solution. All the nanostructures were deposited for 50 s in cyanide-free gold electroplating solution (Metalor, ECF 60, 10 g/L) under -1 mA in a liquid cell with 2.5 cm in diameter.

SEM. SEM images were taken using a field-emission SEM (Zeiss LEO 1550) at 1 kV under 20k×, 30k× and 50k× magnification with stage angle of 0° and 30°.

Sample preparation. The patterned materials were cut into small square discs having a length of 1 cm and placed in 12-well microplates filled with 1 mL 70% ethanol. After 5 min incubation,

ethanol was removed and 1 mL 0.9 % NaCl was immediately added to the wells to prevent sample drying.

Bacteria culture and adhesion. *Staphylococcus aureus* (ATCC 6538) was used in this study. Bacteria from glycerol stocks were grown on Tryptic Soy agar (TSA) plates. Single colony was transferred to 10 mL of tryptic soy broth (TSB) and incubated for overnight at 37 °C. 1 mL of the overnight culture was added to 10 mL fresh TSB and incubated until it has reached late exponential growth phase. The suspension was diluted to an OD600 value of 0.05 with 0.9 % NaCl. 50 µL of the diluted suspension were added to the sterilized discs in 12-well plates and incubated for 2 h at room temperature. Cell suspension was removed and the wells were washed three times with 1 mL 0.9 % NaCl. The samples were either investigated using microscopy or transferred to a new 12-well microplate for proliferation test.

Bacteria viability analysis using fluorescent microscopy. A mixture of 2.5 µM SYTO9 (Life technologies) and 15 µM propidium iodide in 0.9 % NaCl solution was freshly prepared according to manufacturer's instruction and used to stain bacterial cells as described previously[25]. 50 µL of the mixture were added to the top of the sample in a microplate well and the plate was incubated for 30 min at room temperature in the dark. The staining mixture was then removed and the wells with samples were washed three times with 1 mL ddH_2O. The samples were then analyzed with fluorescent microscopy (Leica DM6000B). The laser was used at 488 nm for excitation, and the emission was observed at 528 nm (SYTO9) and 645 nm (PI). For each sample, two independent experiments with three images per sample per experiment were performed. Images were taken at the fixed locations obtain a statistics overview.

Bacteria viability quantification with proliferation test. 250 µL fresh 30 % TSB (9 g/l) was added to each well containing the samples from "Bacterial culture and adhesion" and the plate was incubated for 2 hours. Afterwards 50 µL of the cell culture was taken out and added to a new 96-well plate which contained 150 µL TSB medium. The plate was closed with a sticking transparent foil (Diversified Biotech - Breathe-Easy, T093.1, Carl Roth GmbH+Co. KG) and incubated in a Synergy HT Multi-Detection Microplate Reader (BioTek®) at 37 °C and medium shaking (18Hz - preset value of the instrument). Optical density at 600 nm was measured every 30 min for 12 hours. Under the same conditions with the same bacterial strain, the time taken for bacterial cells to achieve specific OD values is related linearly to the initial viable cell counts, namely, the more viable cells, the shorter time is needed to reach a specific OD value. A dilution series of the bacteria culture enables a correlation between cell numbers and time needed to reach a specific OD. The resulting standard curve was used to calculate the numbers of viable cells on a surface. For each sample, two independent experiments with eight repetitions per sample per experiment were performed. The statistical significance was determined for each data set using the unpaired, parametric, two-tailed t-test.

5. Acknowledgements

S. Wu acknowledges the research funding from the Beijing Jiaotong University (2015RC052).

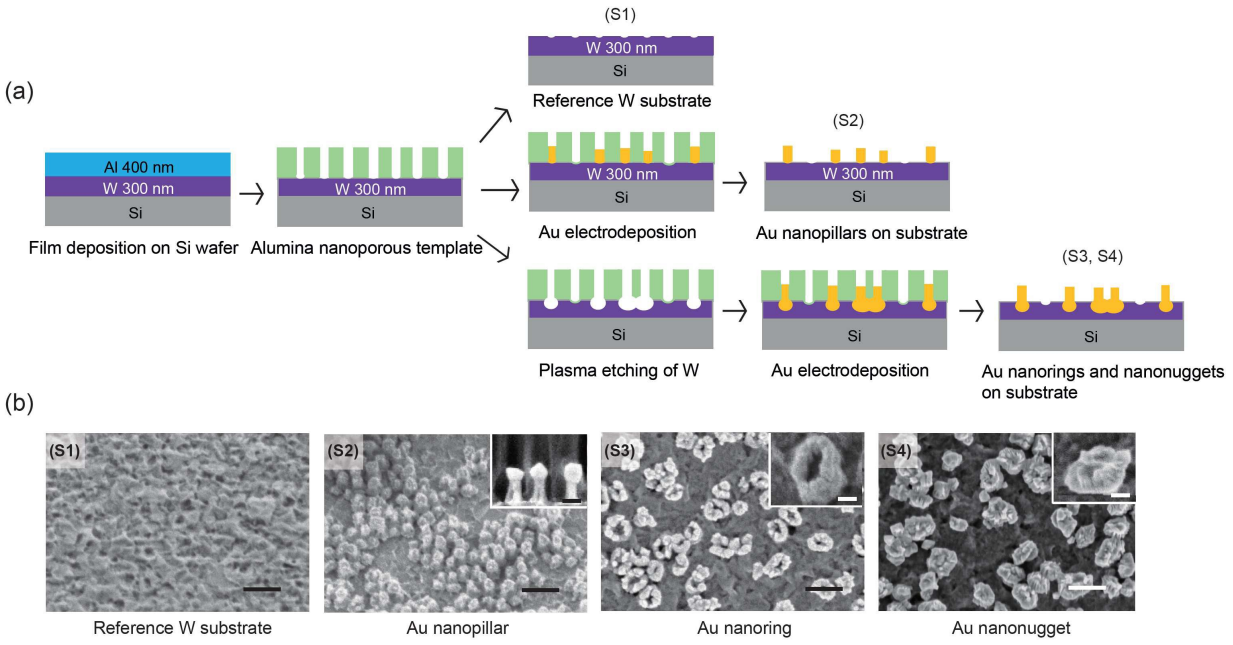

Figure 1. Fabrication and characterization of nanostructured surfaces. (a) Schematic of fabrication process. After the deposition of W and Al thin films, the nanoporous template is generated by Al anodization. Reference W substrate (S1) with nanoscale roughness is obtained by dissolving the alumina nanoporous template. Au nanopillars (S2) are directly electrodeposited using the nanoporous template. Au nanoring (S3) and cluster of nanopillars (S4) are obtained by modifying the structure of the W layer. (b) SEM images of various nanostructured morphologies (scale bar 200 nm). Insect: typical individual nanostructures with scale bar of 50 nm. S1: W reference substrate with nanoscale roughness; S2: Au nanopillars. A typical nanopillar is 50 nm in diameter and 100 nm in height; S3: Au nanorings with outer diameter about 200 nm; S4: Au nanonuggets with diameter about 200 nm.

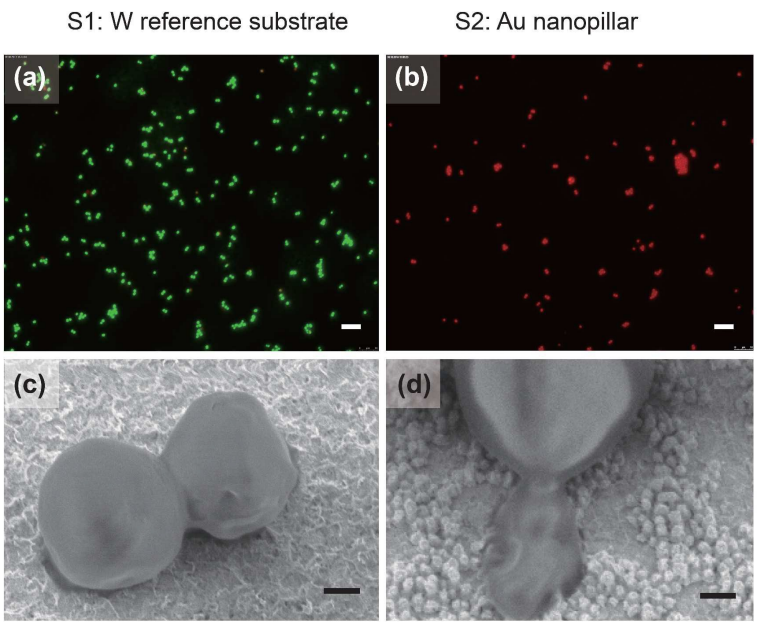

Figure 2. Bactericidal activity of nanostructured gold surfaces. Comparison of fluorescence micrographs of *S. aureus* after 2 hour incubation on reference substrate (S1, a) and nanopillar surface (S2, b). Scale bar: 10 μm. Syto9/PI simultaneously stain cells with intact (Syto9, green) and damaged (PI, red) membranes. For each sample, two independent experiments with three images per sample per experiment were performed. SEM images of *S. aureus* cells on reference substrate (S1, c) and nanopillar surface (S2, d). Scale bar: 200 nm. Deformation and rupture could be seen clearly for the cells on the nanopillar surfaces S2.

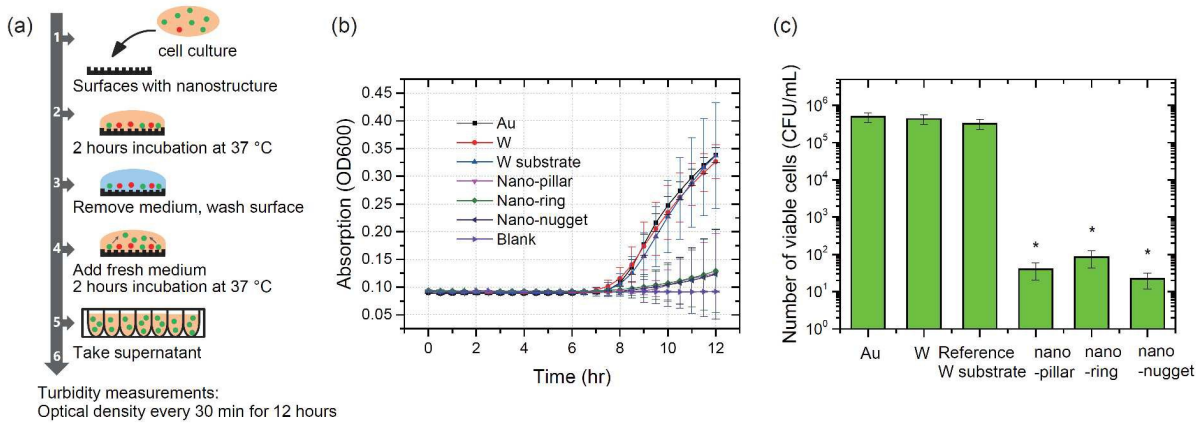

Figure 3. Bactericidal efficiency of nanostructured Au surfaces. (a) Schematic representation of cell proliferation experiments by using various nanostructured surfaces with attached bacteria. The more viable cells on sample surfaces, the faster the cells reach a given OD value. (b) Proliferation curves for the substrate and nanostructured samples with 1×1 cm^2 surface area. (c) Viable cell numbers for different surfaces by extrapolation of the OD value of 0.2 for all the samples. For each sample, two independent experiments with eight repetitions per sample per experiment were performed. Columns are displayed as means, error bars are shown as plus/minus standard error of the mean. The statistical significance was determined for each data set using the unpaired, parametric, two-tailed t-test. *P<0.001 vs. the reference substrate.

Table 1: Summary of antibacterial performance of various nanostructured surfaces tested in this study.

	Diameter (nm)	Height (nm)	Density (/μm^2)	Surface coverage	Bactericidal performance
S1: Reference Substrate	Surface roughness	< 20	-	100 %	Reference
S2: Au nanopillars	~ 50	~100	~ 100	~ 50 %	> 99 %
S3: Au nanorings	100-200, with single pillar ~ 50	~100	~ 30	~ 50 %	> 99 %
S4: Au nanonuggets	100-200, with single pillar ~ 50	~100	~ 30	~ 50 %	> 99 %

References

1. A. J. Scardino, D. Hudleston, Z. Peng, N. A. Paul and R. de Nys, *Biofouling*, 2009, **25**, 83-93.
2. K. Anselme, P. Davidson, A. M. Popa, M. Giazzon, M. Liley and L. Ploux, *Acta Biomaterialia*, 2010, **6**, 3824-3846.
3. L. D. Renner and D. B. Weibel, *Mrs Bulletin*, 2011, **36**, 347-355.
4. A. J. Scardino and R. de Nys, *Biofouling*, 2011, **27**, 73-86.
5. G. D. Bixler and B. Bhushan, *Philos Trans A Math Phys Eng Sci*, 2012, **370**, 2381-2417.
6. A. K. Epstein, D. Hong, P. Kim and J. Aizenberg, *New Journal of Physics*, 2013, **15**.
7. M. V. Graham, A. P. Mosier, T. R. Kiehl, A. E. Kaloyeros and N. C. Cady, *Soft Matter*, 2013, **9**, 6235-6244.
8. M. Graham and N. Cady, *Coatings*, 2014, **4**, 37-59.
9. E. P. Ivanova, J. Hasan, H. K. Webb, V. K. Truong, G. S. Watson, J. A. Watson, V. A. Baulin, S. Pogodin, J. Y. Wang, M. J. Tobin, C. Lobbe and R. J. Crawford, *Small*, 2012, **8**, 2489-2494.
10. J. Hasan, H. K. Webb, V. K. Truong, S. Pogodin, V. A. Baulin, G. S. Watson, J. A. Watson, R. J. Crawford and E. P. Ivanova, *Appl Microbiol Biotechnol*, 2013, **97**, 9257-9262.
11. E. P. Ivanova, J. Hasan, H. K. Webb, G. Gervinskas, S. Juodkazis, V. K. Truong, A. H. F. Wu, R. N. Lamb, V. A. Baulin, G. S. Watson, J. A. Watson, D. E. Mainwaring and R. J. Crawford, *Nat Commun*, 2013, **4**.
12. T. Diu, N. Faruqui, T. Sjöström, B. Lamarre, H. F. Jenkinson, B. Su and M. G. Ryadnov, *Sci. Rep.*, 2014, **4**.
13. J. Hasan, S. Raj, L. Yadav and K. Chatterjee, *RSC Advances*, 2015, **5**, 44953-44959.
14. C. Guo, L. Feng, J. Zhai, G. Wang, Y. Song, L. Jiang and D. Zhu, *Chemphyschem*, 2004, **5**, 750-753.
15. F. X. Zhang and H. Y. Low, *Nanotechnology*, 2006, **17**, 1884-1890.
16. G. Zhang, J. Zhang, G. Xie, Z. Liu and H. Shao, *Small*, 2006, **2**, 1440-1443.
17. P. Roach, N. J. Shirtcliffe and M. I. Newton, *Soft Matter*, 2008, **4**, 224-240.
18. B. Pokroy, A. K. Epstein, M. C. M. Persson-Gulda and J. Aizenberg, *Advanced Materials*, 2009, **21**, 463-469.

19. Y. Engel, J. D. Schiffman, J. M. Goddard and V. M. Rotello, *Materials Today*, 2012, **15**, 478-485.
20. A. I. Hochbaum and J. Aizenberg, *Nano Letters*, 2010, **10**, 3717-3721.
21. S. Pogodin, J. Hasan, V. A. Baulin, H. K. Webb, V. K. Truong, T. H. P. Nguyen, V. Boshkovikj, C. J. Fluke, G. S. Watson, J. A. Watson, R. J. Crawford and E. P. Ivanova, *Biophysical Journal*, 2013, **104**, 835-840.
22. A. M. Whatmore and R. H. Reed, *J. Gen. Microbiol.* , 1990, **136**, 2521–2526.
23. S. Wu, F. Wildhaber, A. Bertsch, J. Brugger and P. Renaud, *Applied Physics Letters*, 2013, **102**, 213108.
24. H. Masuda, H. Yamada, M. Satoh, H. Asoh, M. Nakao and T. Tamamura, *Applied Physics Letters*, 1997, **71**, 2770-2772.
25. P. Stiefel, S. Schmidt-Emrich, K. Maniura-Weber and Q. Ren, *BMC Microbiology*, 2015, **15**, 36.